Temperature-Bias Compensation of Low-Cost Inertial Sensors – Possible or Pipe Dream?

Authors: Dariusz Maton, John T. Economou, David Galvão Wall, Irfan Khan, Robert Cooper, David Ward, Simon Trythall.

Abstract:

Navigation using low-cost inertial sensors costing less than £1 each is generally considered impossible. With various measurement error contributions, the velocity and position estimates from these sensors drift exponentially with time. By simulating the sensor, we show how the zero bias error is the most serious contributor. The zero bias is known to change with temperature due to dissimilar thermomechanical characteristics of materials in the sensor's construction and others have shown this trend to be nonlinear, exhibit hysteresis and unique to each sensor. This is a problem because it suggests error compensation by modelling (software level), or sensor redundancy (hardware level) will be ineffective. From temperature experiments on three of the same low-cost sensors, we show that temperature-bias responses are indeed unique and nonlinear but may be opposing between sensors. Furthermore, we show that one can get lucky and obtain a sensor with an axis that is relatively insensitive to temperature. This is encouraging because it supports the idea that an inertial measurement unit comprised of an array of inertial sensors can be fused to provide higher accuracy measurements than a single sensor operating alone. Lastly, we identify a threat to this idea we call temperature shock and suggest how it can be avoided. While the contributions of this work are intended to improve the accuracy of human position tracking, their impact extends to any field where lengthy periods of position tracking under Global Positioning System (GPS) denial is required.

1. Introduction

Tracking the positions of humans and vehicles in GPS denied environments is in ever-increasing demand. By 2050 for example, more than two thirds of the world's population will inhabit built-up areas where multipath and signal fading can interfere with measurements crucial for localisation (Ritchie & Roser, 2018). A lack of accurate position tracking of emergency responders can be particularly serious and, in some cases, have fatal consequences (Anderson, 1999; Fire Brigades Union, 2007). The vulnerability of GPS to spoofing and jamming is also a concern in the use of uninhabited aerial systems (UASs) for maritime patrol and critical infrastructure inspection (C4ADS, 2019; Lee et al., 2016).

1.1 Alternative Technologies

Ultrawideband (UWB) position tracking systems are an attractive GPS alternative. Their signals are difficult to detect and jam by operating close to the noise floor power level, give positioning with decimetre accuracy and have operating ranges of several 100s of metres (Gunia et al., 2016; Jimenez Ruiz & Seco Granja, 2017). However, like positioning systems that use visible fiducials (Bhargavapuri et al., 2019), photodiodes (Sitole et al., 2020; Welch et al., 2001), radio frequency identification (RFID) (De Cillis et al., 2020) and wireless fidelity (Wi-Fi) (Woodman & Harle, 2009), they require pre-deployment of certain components into the environment for their operation. In many situations where ad hoc tracking is required, this is not a practical approach.

Although visual odometry (VO) systems are capable of tracking natural features (Nabavi-Chashmi et al., 2023), there are circumstances where such features are not visible in the camera frame such as operating in poorly lit environments like mines (Kanellakis & Nikolakopoulos, 2016). Other cases where VO may fail include edge-case operating conditions such as foggy (Bijelic et al., 2019), smoky (Saputra

et al., 2019) and dusty environments (Khattak et al., 2019). While thermal imaging cameras have been used by firefighters for improving situational awareness, use around fuel and petroleum fires has been reported to hinder their efficacy (Fire Brigades Union, 2007).

1.2 Inertial Sensors

Compared with the mentioned technologies, inertial sensors are self-contained sensors, meaning they operate independently of any supporting infrastructure (Noureldin et al., 2013). This is because they use Newton's laws which are ever-present. Inertial sensors generally refer to accelerometers and gyroscopes, measuring specific force and angular velocity of the sensor frame relative to the inertial reference frame. Inertial measurement units (IMUs) usually contain triads of mutually orthogonal accelerometers and gyroscopes and, thanks to micro-electromechanical systems (MEMS) manufacturing, low-cost, lightweight, low power IMUs can be found in most electronic devices. Unlike GPS however, position cannot be estimated in an absolute sense but relative to a known initial position by a process of dead reckoning (Verplaetse, 1996). This is a problem as, conventionally, the current position estimate is derived from a cumulative sum of the previous measurements (integration) which may be sampled a few hundred times every second. Thus, even small measurement errors accumulate in the estimated position resulting in divergence from the true position. Although this rate of divergence is sufficiently small for navigation and strategic grade sensors, these are orders of magnitude more expensive and not commercially available off the shelf (Yole Developpement, 2020). Figure 1 shows a commercial off the shelf inertial sensor package.

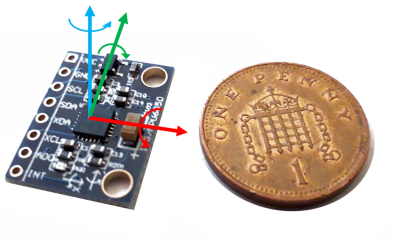

Figure 1. An MPU-6050 inertial sensor.

The measurement errors mentioned can be random or systematic. As random errors are assumed to be uncorrelated in time and unpredictable, the focus of this work is on the latter.

1.3 Systematic Inertial Sensor Errors

Table 1 shows the systematic errors commonly cited in low-cost inertial sensor datasheets.

Table 1. Systematic sensor errors for low-cost inertial sensors.

Sensor error:	Description:	Cause:
Zero bias	The offset in the measurement when no input is applied.	Materials with dissimilar thermomechanical characteristics used in construction (Zhang et al., 2007).
Scale factor	The multiplicative term relating the change in the output signal to the change in the measured input.	Temperature changing the stiffness of sensor's flexures.
Cross-axis sensitivity	Nonorthogonality and misalignment of the sensor axes.	Manufacturing imperfections (Hiller et al., 2021).

While datasheets for low-cost IMUs such as the MPU-6050 provide figures for typical zero bias, scale factor and cross-axis sensitivity errors, it is unclear which of these is the biggest contributor and hence the most worthy of compensation.

While zero bias and scale factor errors can be compensated using routines such as those in (Glueck et al., 2014), these will become invalid as the sensor temperature changes. This can be caused by changes in the ambient temperature or sensor self-heating as show in Figure 2.

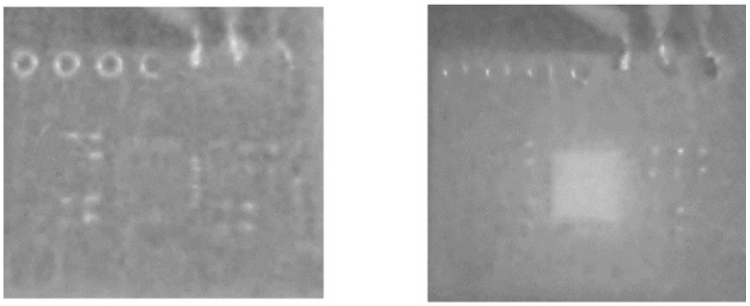

(a) (b)

Figure 2. MPU-6050 under thermal camera. (a) off, (b) on.

Two approaches to temperature compensation in literature are either hardware or software based.

Software based solutions involve modelling the temperature-bias response to apply compensation afterwards. In (Khankalantary et al., 2021) and (Gang-Qiang et al., 2023), mathematical models were proposed to compensate for the bias variation but did not address the issue of hysteresis. (Vandemeer et al., 2003) acknowledged hysteresis in the bias as the most important temperature dependent behaviour as it is complex, having both memory and direction dependence. Although their proposed model showed promising experimental results, performance under sudden temperature changes was not explored.

Hardware based solutions such as those in (Lemmerhirt et al., 2019; Yang et al., 2017) involve the addition of a temperature control system to ensure the sensor remains at a constant temperature during operation. Although improvements in the bias were demonstrated, they rely on specialised electronics manufacturing techniques in their implementations. A low-cost hardware-based approach investigated by (Martin et al., 2013; Yuksel et al., 2010) proposed placing sensors with correlated temperature-bias responses with their axes opposing such that the average measurement nulls the error. In doing so, the error compensation task focusses less on trying the predict the temperature bias response of the sensors, and rather seeks to find sensors that have similar or opposing responses.

This work builds on this idea by investigating the temperature-bias responses from multiple low-cost MPU-6050 inertial measurement units.

The contributions of this work are thus:

- The modelling of an accelerometer to identify the most significant measurement error source.
- Displaying the temperature-bias response from three of the same IMUs, suggesting intelligent fusion that may enable compensation.
- An investigation of the effects of humidity and sudden temperature changes on sensor biases.

2. Method

2.1 Identification of the most significant measurement error.

To identify the most significant error in the inertial sensor measurements, a three-axis accelerometer was modelled in MATLAB shown in Figure 3 with error sources highlighted in red.

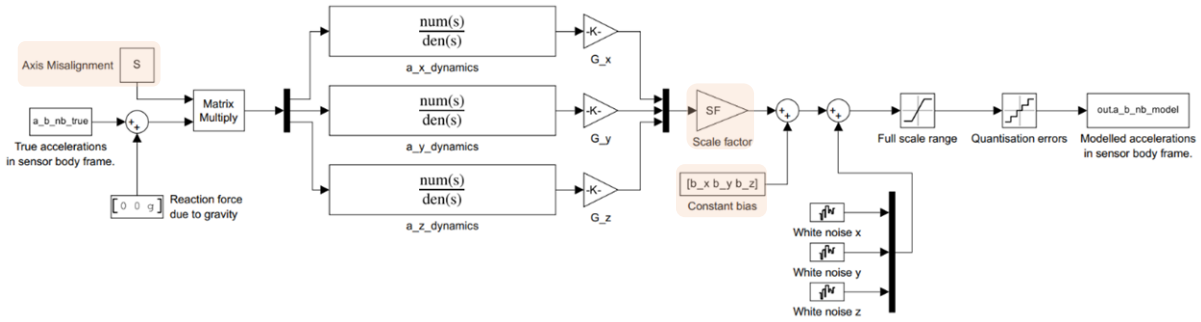

Figure 3. Three-axis accelerometer model.

Inputs to the model were ideal sensed accelerations corresponding to the sensor traversing a flat rounded-square path measuring 1.5 m x 1.5 m. Individual error contributions were then added to the sensor model according to their description in the MPU-6050 sensor's datasheet.

2.2 Temperature-bias Experiments

For obtaining the temperature-bias responses of the inertial sensors, a Sanyo Gallenkamp environmental chamber was used which allowed control of temperature and humidity.

The inertial sensors were mounted onto a breadboard which was approximately levelled using an inclinometer. Supporting electronic components were mounted outside of the working area of the chamber wherever possible to ensure the responses observed were due to temperature variations of the sensors themselves. Figure 4 shows the chamber and sensor setup.

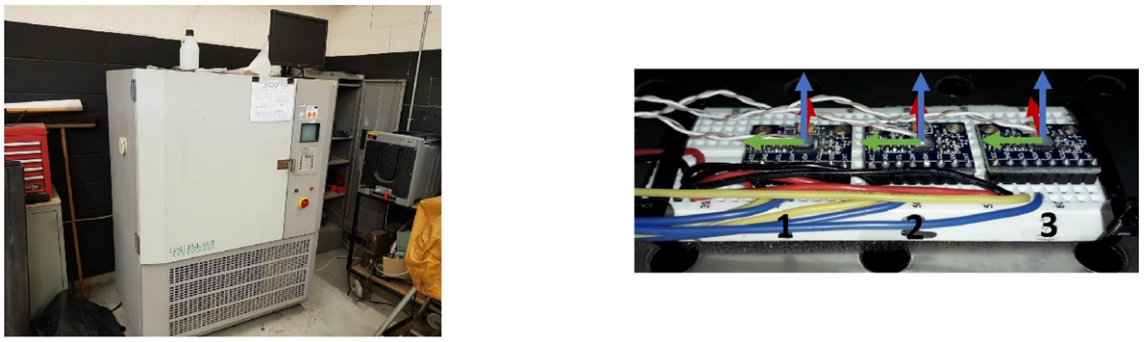

(a) (b)

Figure 4. (a) Environmental chamber, (b) setup of multiple inertial sensors.

Four experiments carried out in the chamber were: a sweep across the sensor's operating range (-20°C to 70°C), cycles between 0°C and 20°C, a linear decrease in relative humidity from 90% to 20% for a constant temperature of 35°C and a sudden change in the rate of temperature change. The temperature sweep experiment was carried out to validate the extent of the temperature-bias

variation quoted in the MPU-6050 datasheet, the temperature cycling experiment simulated the effect of walking between indoor and outdoor environments and the humidity test was a curiosity to see if humidity influenced sensor biases. The last experiment was inspired by the warning against sudden temperature changes reported in (Vandemeer et al., 2003).

3. Results

3.1 Assessment of various systematic error sources

Table 2 shows the sensor errors added and their effect on mean squared acceleration error, a_{mse}.

Table 2. Sensor errors added to the accelerometer model.

Sensor error:	Description in datasheet:	a_{mse} (ms^{-2}):
Zero bias	±40mg (between 0°C and 70°C)	0.134
Scale factor	±1.4% (between 0°C and 70°C)	0.030
Cross-axis sensitivity	±2%	0.042

3.2 Experimental Results using Environmental Chamber

Figure 5 shows the results of the temperature sweep experiment. In this experiment, relative humidity was treated as a free variable.

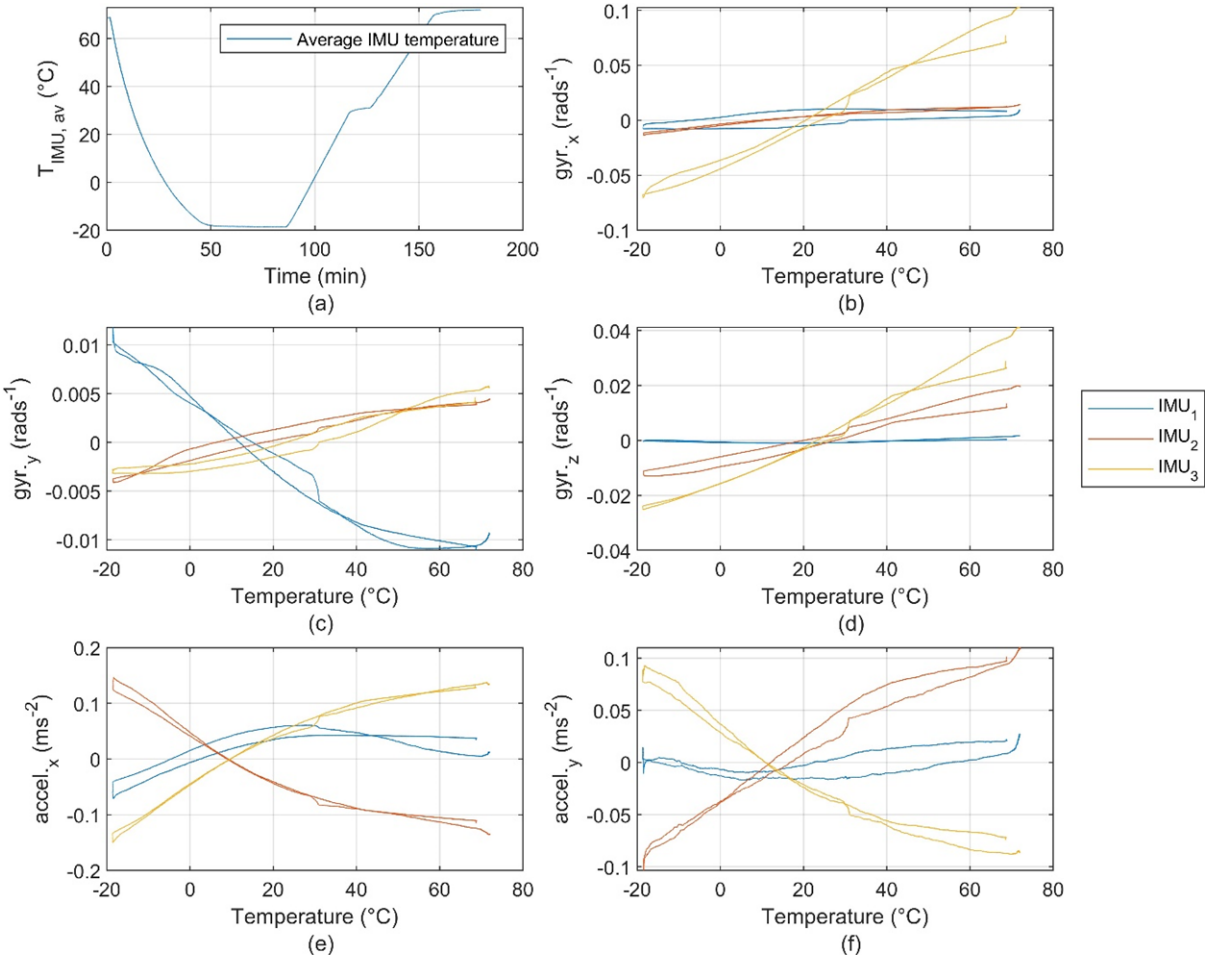

Figure 5. (a) Temperature time plot, (b) gyro x-axis bias plot, (c) gyro y-axis bias plot, (d) gyro z-axis bias plot, (e) accelerometer x-axis bias plot and (f) accelerometer y-axis bias plot.

Figure 6 shows temperature and bias variation for three cycles of the chamber temperature between 0°C and 20°C. As in the previous experiment, humidity was not controlled.

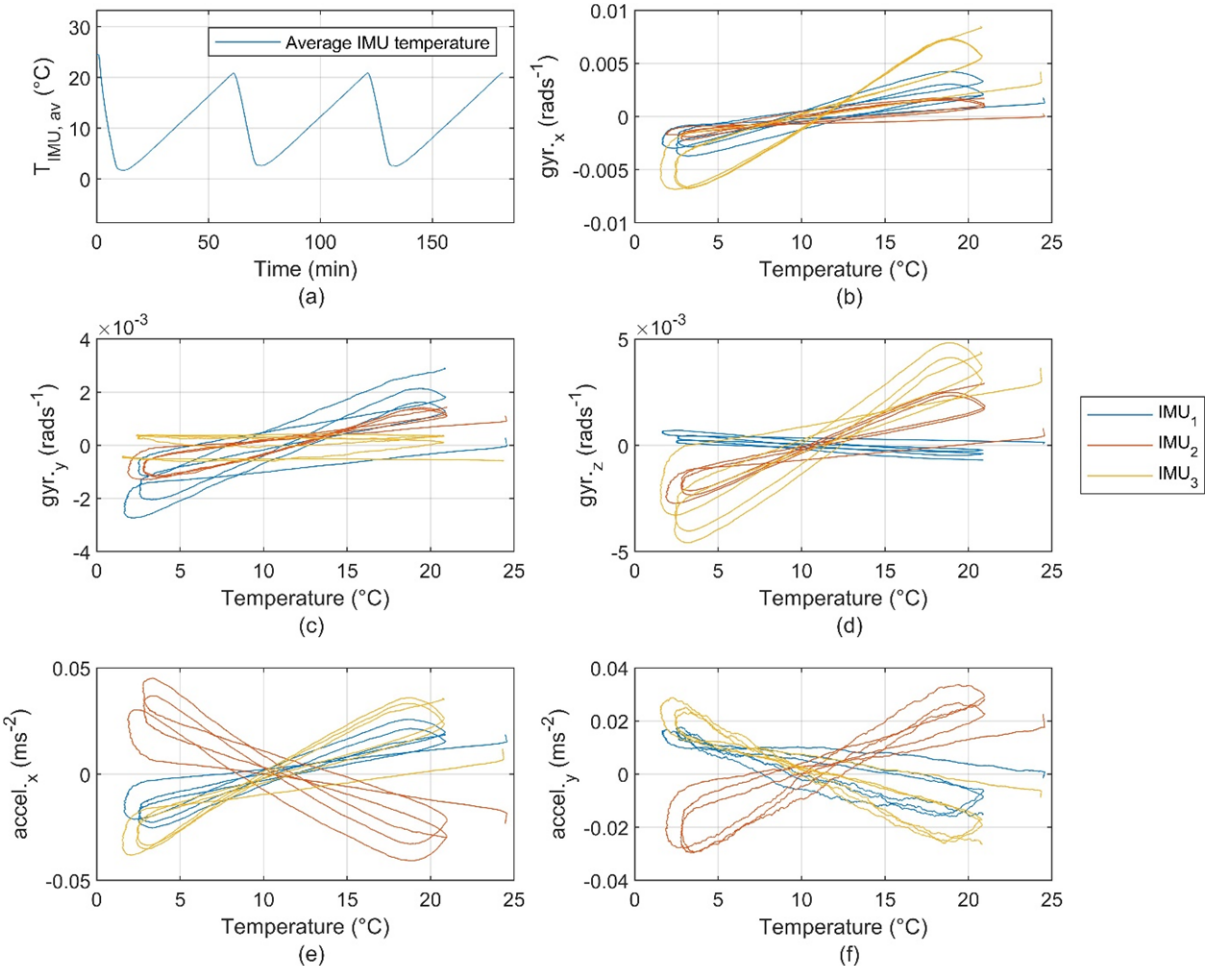

Figure 6. (a) Temperature time plot, (b) gyro x-axis bias plot, (c) gyro y-axis bias plot, (d) gyro z-axis bias plot, (e) accelerometer x-axis bias plot and (f) accelerometer y-axis bias plot.

Figure 7, shows the bias variation in three inertial sensors for an approximately linear decrease in humidity from 90% to 20% over four hours. A constant temperature of 35°C was maintained with deviation less than ±0.5°C over this run.

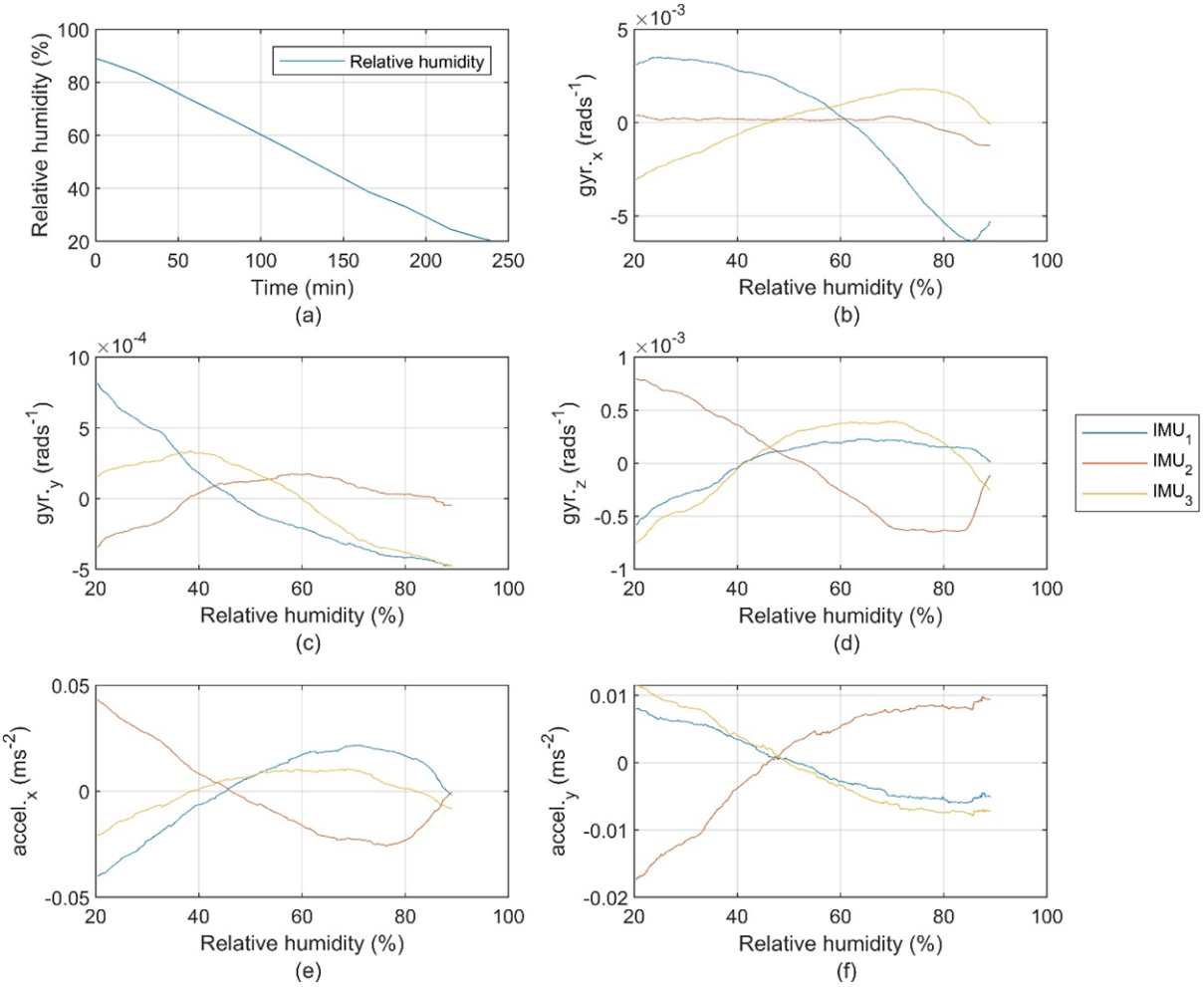

Figure 7. (a) Relative humidity-time plot, (b) gyro x-axis bias plot, (c) gyro y-axis bias plot, (d) gyro z-axis bias plot, (e) accelerometer x-axis bias plot and (f) accelerometer y-axis bias plot.

Lastly, Figure 8 shows the bias variation of each axis of the inertial sensor for a sudden change in the rate of change of temperature.

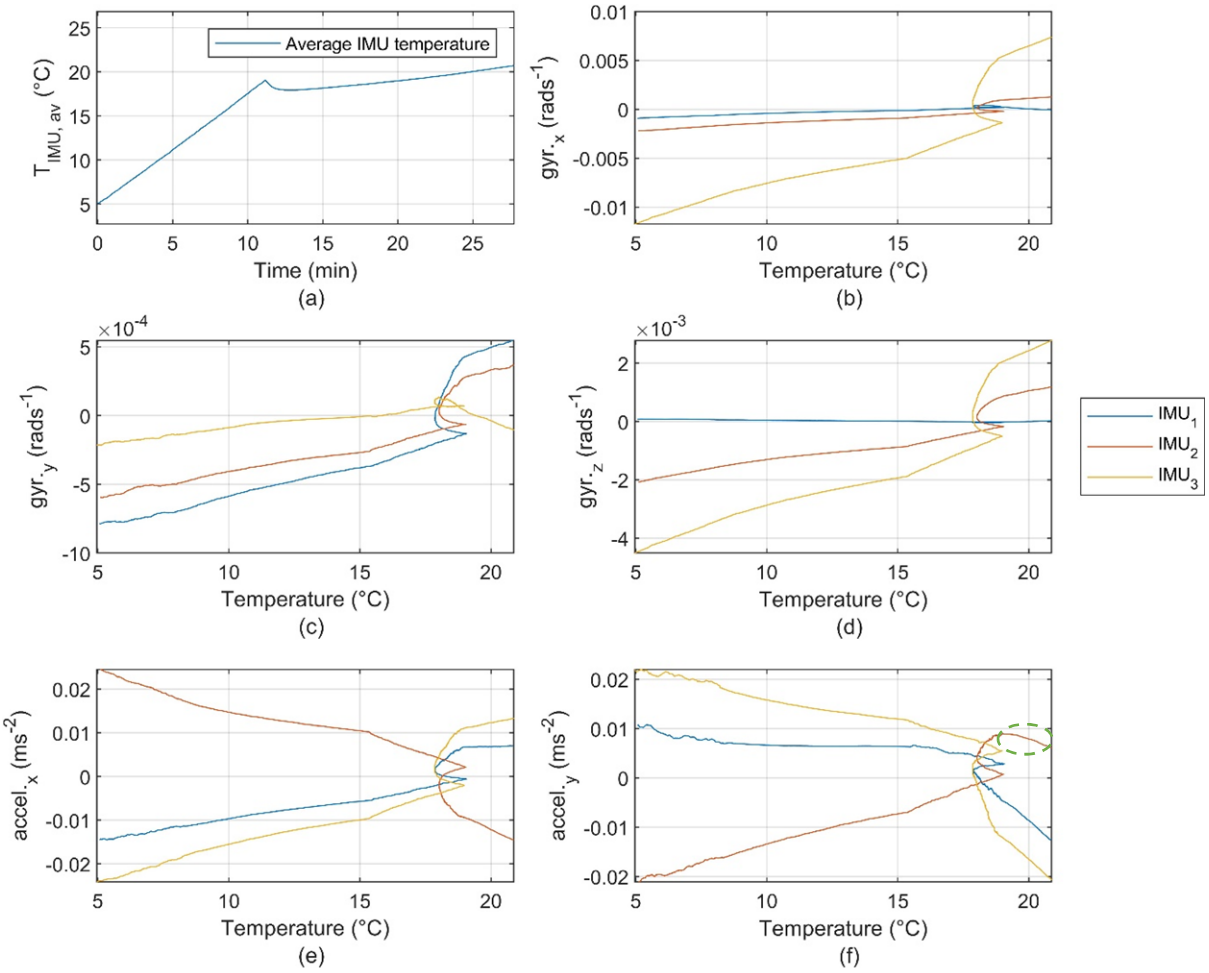

Figure 8. (a) Time plot, (b) gyro x-axis bias plot, (c) gyro y-axis bias plot, (d) gyro z-axis bias plot, (e) accelerometer x-axis bias plot and (f) accelerometer y-axis bias plot.

4. Discussion

The mean squared acceleration errors shown in Table 1 suggest that the zero bias error is the most significant error contributor to the accelerometer measurements, giving mean squared velocity errors approximately four times larger than the errors in scale factor and misalignment.

The temperature-bias plots for the sweep over the sensor's operating range in Figure 5 shows the variability in responses between the sensors and their axes. This variability is greater in the gyroscopes than the accelerometers. Of the gyroscopes, the x-axis of IMU 3 showed the largest bias, reaching a maximum value of 0.1 rads^{-1} corresponding to 2.3% of the full-scale range of the sensor. In contrast, the z-axis gyroscope of IMU 1 (Figure 5(d)) reached a maximum bias of 0.0017 rads^{-1} (about 60 times lower). The same variability in responses was not observed between accelerometers where a maximum bias of about 0.13 ms^{-2} was attained (corresponding to 0.7% of full-scale range) compared with a minimum of 0.025 ms^{-2} (about 4 times lower). Interestingly, the accelerometer responses between IMUs 2 and 3 appeared as reflections in the temperature axis suggesting that there may be some utility in their fusion as a means of nulling the error. Figure 9 shows what the effect of this could be for this experiment where bias variation is reduced approximately sevenfold as a result. The cause of these opposing responses is hypothesised to be due to differences in orientation of the individual

accelerometers on the MEMS chip during manufacture. This could be confirmed by decapsulating the sensors and looking at their structure under a microscope.

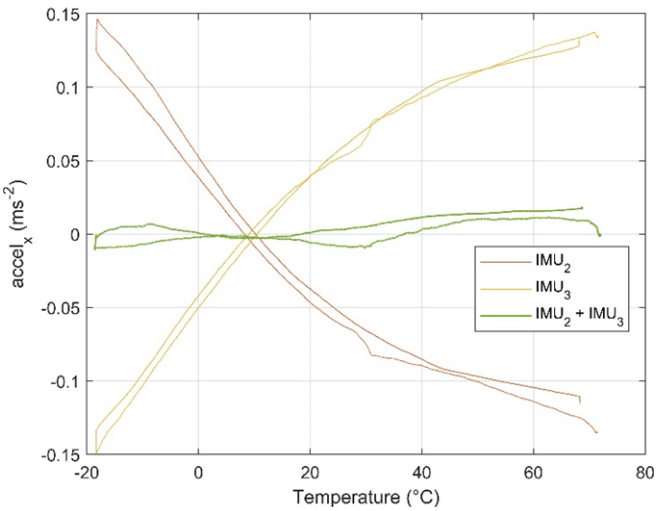

Figure 9. Effect of fusing responses from IMUs 2 and 3 for the temperature sweep experiment.

The thermal cycling plots in Figure 6 show the repeatability problem in the responses and why a simple polynomial fit may become ineffective as a means of compensation. The bow-tie shaped plots do not directly overlap and instead, appear translated and skewed between thermal cycles. This supports what has been reported previously in literature that bias responses resemble hysteresis loops whose size is governed by the range of temperatures and their rate of change.

The results in Figure 7 show how humidity also affects inertial sensor zero biases. In the worst cases, bias varied by 0.005 rads^{-1} in the gyros (0.1% of full scale range) and 0.05 m/s2 (about 0.25% of the full scale range) in the accelerometers. Humidity thus appears to affect the accelerometer biases more than the gyroscope biases. The details of the gyroscope's construction in (Seeger et al., 2010), suggest that this could be because the gyroscopes are hermetically sealed but the accelerometers are not. Humidity may be a cause for the repeatability problem seen in the thermal cycling. Future work will therefore hermetically seal one the sensor packages using epoxy resin and observe the resulting response to thermal cycling to see if an improvement in repeatability can be achieved. Referring to Figure 7(e) and (f) it can be seen how IMUs 2 and 3 also have opposing responses to humidity.

Lastly, in Figure 8 the effect of a sudden change in the rate of change of temperature at 11 minutes is observed. In Figure 8(b) and (d), the gyroscope axes of IMU 1 are seen to have no discernible impact on bias despite the sudden change in rate. This demonstrates the worth of performing such experiments as sensors with more desirable characteristics can be identified from even a small batch (in this case of only three sensors). While in previous experiments, the opposing nature of responses from IMUs 2 and 3 were noted with a view of using this to null the temperature induced bias error, the sudden change in the rate of change of temperature may cause this compensation technique to fail. Referring to Figure 8(f), while IMUs 2 and 3 initially had opposing responses, after the sudden change in rate, the response of IMU 2 has the same direction as that of IMU 3 (region circled green). The errors may therefore become reinforced instead of nulled as a result. This may be avoided by adding thermal inertia to the sensors such that they do not experience these sudden temperature changes.

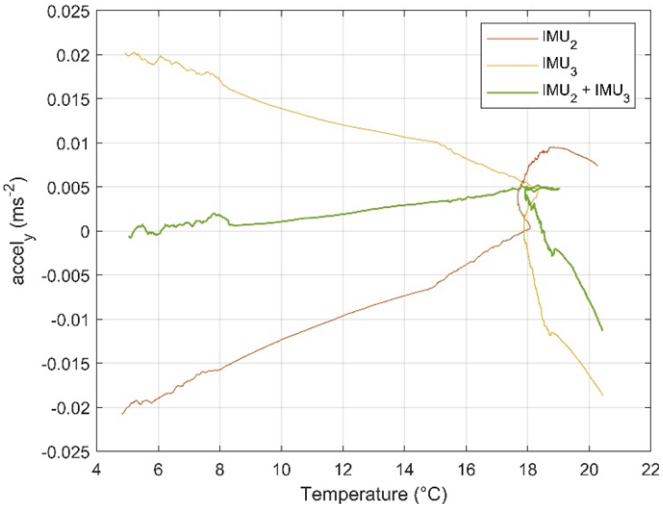

Figure 10. Effect of fusing responses from IMUs 2 and 3 for the sudden change in rate of temperature change.

5. Conclusion

This work explored the measurement errors affecting low-cost inertial sensors, specifically the MPU-6050 was subject to investigation.

Simulation of accelerometers with typical temperature-induced bias errors demonstrated how it resulted in a larger measurement error compared with scale factor and axis misalignment errors.

Based on the data from the three IMUs, the experiments demonstrated how:

- The sensor-to-sensor temperature bias responses varied approximately 15 times more between the gyroscopes than the accelerometers. One gyroscope was found to have an attractive flat temperature-bias response.
- Certain accelerometer axes had opposing temperature-bias responses suggesting their summation could help reduce the error by as much as sevenfold.
- The accelerometers were affected more by humidity than the gyroscopes. Those sensors with opposing temperature-bias responses also had opposing humidity-bias responses suggesting their fusion may help compensate for humidity effects as well as temperature.
- Sudden changes in the rate of temperature change should be avoided in such a fusion scheme as it may cause opposing responses to become correlated which would reinforce the bias error. Adding thermal inertia to the sensor structure may help avoid this.

6. Acknowledgements

This work was supported by EPSRC iCASE Grant EP/S513623/1 and BAE Systems.

7. Data Availability Statement

Data supporting this study are openly available from CORD at 10.17862/cranfield.rd.24291112.

8. References

Anderson, J. R. (1999). *Abandoned Cold Storage Warehouse Multi-Firefighter Fatality Fire* (Issue December). https://www.usfa.fema.gov/downloads/pdf/publications/tr-134.pdf

Bhargavapuri, M., Shastry, A. K., Sinha, H., Sahoo, S. R., & Kothari, M. (2019). Vision-based autonomous tracking and landing of a fully-actuated rotorcraft. *Control Engineering Practice*, *89*, 113–129. https://doi.org/10.1016/j.conengprac.2019.05.015

Bijelic, M., Gruber, T., Mannan, F., Kraus, F., Ritter, W., Dietmayer, K., & Heide, F. (2019). *Seeing Through Fog Without Seeing Fog: Deep Multimodal Sensor Fusion in Unseen Adverse Weather*. http://arxiv.org/abs/1902.08913

C4ADS. (2019). *Exposing GPS Spoofing in Russia and Syria.* https://static1.squarespace.com/static/566ef8b4d8af107232d5358a/t/5c99488beb39314c45e782da/1553549492554/Above+Us+Only+Stars.pdf

De Cillis, F., Faramondi, L., Inderst, F., Marsella, S., Marzoli, M., Pascucci, F., & Setola, R. (2020). Hybrid Indoor Positioning System for First Responders. *IEEE Transactions on Systems, Man, and Cybernetics: Systems*, *50*(2), 468–479. https://doi.org/10.1109/TSMC.2017.2772821

Fire Brigades Union. (2007). *Fatal Accident Investigation - Full report Into the deaths of firefighters John Averis , Ian Reid, Ashley Stephens and Darren Yates-Badley* (Issue November). https://www.ife.org.uk/write/MediaUploads/Incident directory/Atherstone - 2007/Atherstone_FBU_Report_Full_Redacted.PDF

Gang-Qiang, G., Bo, C., Rui-Chu, C., & Yun-Shuang, W. (2023). Real-Time Temperature Drift Compensation Method of a MEMS Accelerometer Based on Deep GRU and Optimized Monarch Butterfly Algorithm. *IEEE Access*, *11*, 10355–10365. https://doi.org/10.1109/ACCESS.2023.3240766

Glueck, M., Oshinubi, D., Schopp, P., & Manoli, Y. (2014). Real-Time Autocalibration of MEMS Accelerometers. *IEEE Transactions on Instrumentation and Measurement*, *63*(1), 96–105. https://doi.org/10.1109/TIM.2013.2275240

Gunia, M., Protze, F., Joram, N., & Ellinger, F. (2016). Setting up an Ultra-Wideband positioning system using off-the-shelf components. *2016 13th Workshop on Positioning, Navigation and Communications (WPNC)*, 1–6. https://doi.org/10.1109/WPNC.2016.7822860

Hiller, T., Blocher, L., Vujadinovic, M., Pentek, Z., Buhmann, A., & Roth, H. (2021, March 22). Analysis and Compensation of Cross-Axis Sensitivity in Low-Cost MEMS Inertial Sensors. *INERTIAL 2021 - 8th IEEE International Symposium on Inertial Sensors and Systems, Proceedings*. https://doi.org/10.1109/INERTIAL51137.2021.9430454

Jimenez Ruiz, A. R., & Seco Granja, F. (2017). Comparing Ubisense, BeSpoon, and DecaWave UWB Location Systems: Indoor Performance Analysis. *IEEE Transactions on Instrumentation and Measurement*, *66*(8), 2106–2117. https://doi.org/10.1109/TIM.2017.2681398

Kanellakis, C., & Nikolakopoulos, G. (2016). Evaluation of visual localization systems in underground mining. *24th Mediterranean Conference on Control and Automation, MED 2016*, 539–544. https://doi.org/10.1109/MED.2016.7535853

Khankalantary, S., Ranjbaran, S., & Ebadollahi, S. (2021). Simplification of calibration of low-cost MEMS accelerometer and its temperature compensation without accurate laboratory

equipment. *Measurement Science and Technology*, *32*(4). https://doi.org/10.1088/1361-6501/abd0bf

Khattak, S., Papachristos, C., & Alexis, K. (2019). *Visual-Thermal Landmarks and Inertial Fusion for Navigation in Degraded Visual Environments*. https://doi.org/10.1109/AERO.2019.8741787

Lee, Y. S., Kang, Y.-J., Lee, S.-G., Lee, H., & Ryu, Y. (2016). *An Overview of Unmanned Aerial Vehicle: Cyber Security Perspective*. 13. https://doi.org/10.21742/asehl.2016.4.30

Lemmerhirt, D., Srivannavit, O., Chen, S., Litow, T., Mitchell, J., Cooksey, P. C., Sturdevant, R., Bingham, J., Padilla, O., & Trevino, M. N. (2019). Improved Scale-Factor and Bias Stability of Ovenized Inertial Sensors in an Environmentally-Stabilized Inertial Measurement Unit (eIMU). *2019 IEEE International Symposium on Inertial Sensors and Systems (INERTIAL)*, 1–4. https://doi.org/10.1109/ISISS.2019.8739649

Martin, H., Groves, P., Newman, M., & Faragher, R. (2013). A new approach to better low-cost MEMS IMU performance using sensor arrays. *Proceedings of the 26th International Technical Meeting of The Satellite Division of the Institute of Navigation (ION GNSS 2013)*.

Nabavi-Chashmi, S. Y., Asadi, D., & Ahmadi, K. (2023). Image-based UAV position and velocity estimation using a monocular camera. *Control Engineering Practice*, *134*. https://doi.org/10.1016/j.conengprac.2023.105460

Noureldin, A., Karamat, T. B., & Georgy, J. (2013). *Fundamentals of Inertial Navigation, Satellite-based Positioning and their Integration*. Springer Berlin Heidelberg. https://doi.org/10.1007/978-3-642-30466-8

Ritchie, H., & Roser, M. (2018). Urbanization. *Our World in Data*. https://ourworldindata.org/urbanization

Saputra, M. R. U., de Gusmao, P. P. B., Lu, C. X., Almalioglu, Y., Rosa, S., Chen, C., Wahlström, J., Wang, W., Markham, A., & Trigoni, N. (2019). *DeepTIO: A Deep Thermal-Inertial Odometry with Visual Hallucination*. http://arxiv.org/abs/1909.07231

Seeger, J., Lim, M., & Nasiri, S. (2010). Development of High-Performance, High-volume Consumer MEMS Gyroscopes. *2010 Solid-State, Actuators, and Microsystems Workshop Technical Digest*, 61–64. https://doi.org/10.31438/trf.hh2010.16

Sitole, S. P., Lapre, A. K., & Sup, F. C. (2020). Application and Evaluation of Lighthouse Technology for Precision Motion Capture. *IEEE Sensors Journal*, *20*(15), 8576–8585. https://doi.org/10.1109/JSEN.2020.2983933

Vandemeer, J. E., Li, G., & Mcneil, A. C. (2003). Analysis of thermal hysteresis on micromachined accelerometers. *Proceedings of IEEE Sensors 2003 (IEEE Cat. No.03CH37498)*, 1235–1238. https://doi.org/10.1109/ICSENS.2003.1279142

Verplaetse, C. (1996). Inertial proprioceptive devices: Self-motion-sensing toys and tools. *IBM Systems Journal*, *35*(3–4), 639–650.

Welch, G., Bishop, G., Vicci, L., Brumback, S., Keller, K., & Colucci, D. (2001). High-Performance Wide-Area Optical Tracking: The HiBall Tracking System. *Presence: Teleoperators and Virtual Environments*, *10*(1), 1–21. https://doi.org/10.1162/105474601750182289

Woodman, O., & Harle, R. (2009). RF-Based Initialisation for Inertial Pedestrian Tracking. In *Lecture Notes in Computer Science (including subseries Lecture Notes in Artificial Intelligence and Lecture Notes in Bioinformatics): Vol. 5538 LNCS* (pp. 238–255). https://doi.org/10.1007/978-3-642-01516-8_17

Yang, D., Woo, J. K., Lee, S., Mitchell, J., Challoner, A. D., & Najafi, K. (2017). A Micro Oven-Control System for Inertial Sensors. *Journal of Microelectromechanical Systems*, *26*(3), 507–518. https://doi.org/10.1109/JMEMS.2017.2692770

Yole Developpement. (2020). *High-End Inertial Sensors for Defence, Aerospace & Industrial Applications*. https://s3.i-micronews.com/uploads/2020/02/YDR20063-High-End-Inertial-Sensors-2020-Sample.pdf

Yuksel, Y., El-Sheimy, N., & Noureldin, A. (2010). Error Modelling and Characterisation of Environmental Effects for Low Cost Inertial MEMS Units. *IEEE/ION Position, Location and Navigation Symposium*, 598–612. https://doi.org/10.1109/PLANS.2010.5507180

Zhang, X., Park, S., & Judy, M. W. (2007). Accurate assessment of packaging stress effects on MEMS sensors by measurement and sensor-package interaction simulations. *Journal of Microelectromechanical Systems*, *16*(3), 639–649. https://doi.org/10.1109/JMEMS.2007.897088